Journal of Power Sources 263 (2014) 130–140

Contents lists available at ScienceDirect

Journal of Power Sources

journal homepage: www.elsevier.com/locate/jpowsour

Influence of electrolyte ion–solvent interactions on the performances of supercapacitors porous carbon electrodes

C. Decaux [a], C. Matei Ghimbeu [b], M. Dahbi [c], M. Anouti [c], D. Lemordant [c], F. Béguin [d], C. Vix-Guterl [b], E. Raymundo-Piñero [a,e,*]

[a] Centre de Recherche sur la Matière Divisée, CNRS – Université, 1b Rue de la Férollerie, 45071 Orléans, France
[b] Institut de Science des Matériaux de Mulhouse (IS2M), UMR-7361 CNRS – UHA, 15, rue Jean Starcky, BP 2488, 68057 Mulhouse, France
[c] Université François-Rabelais, Physicochimie des matériaux et électrolytes pour l'énergie, PCM2E (EA 6299), Fac Sci & Tech, F-37200 Tours, France
[d] Institute of Chemistry and Technical Electrochemistry, Poznan University of Technology, Piotrowo 3, 60-965 Poznan, Poland
[e] CNRS, CEMHTI UPR3079, Univ. Orléans, F-4071 Orléans, France

HIGHLIGHTS

- A series of porous carbons with tuneable porous texture were prepared.
- Performance of carbon supercapacitors were evaluated in different electrolytes.
- Relationship between porous texture and solvent–salt interaction was studied.
- Highly polarizing ions in polar solvents do not completely loss the solvation shell.
- The optimal carbon pore size depends on the solvent-ion couple used as electrolyte.

ARTICLE INFO

Article history:
Received 30 October 2013
Received in revised form
28 March 2014
Accepted 6 April 2014
Available online 18 April 2014

Keywords:
Supercapacitors
Organic electrolytes
Porous carbon
Ion solvation
Alkylcarbonates
Acetonitrile

ABSTRACT

The development of advanced and safe electrochemical supercapacitors or hybrid supercapacitors combining a battery electrode material such as graphite and a porous carbon electrode implies the use of new electrolytes containing a tetra-alkylammonium or lithium salt dissolved preferentially in a safe and environmentally friendly solvent such as alkylcarbonates. In those systems, the carbon porosity of the activated carbon electrode controls the electrochemical behavior of the whole device. In this work, it is demonstrated that electrolytes containing highly polarizing ions such as Li^+ dissolved in polar solvents such as alkylcarbonates do not completely loss their solvation shell at the opposite of what is observed for poorly solvated cations like $TEABF_4$. As a consequence, the optimal carbon pore size for obtaining the largest energy density, while keeping a high power density, is wider when strongly solvated cations, like Li^+ are used than for conventional organic electrolytes using acetonitrile as solvent and TEA^+ as salt cations. TEA^+ cations are easily desolvated and hence are able to penetrate in small pores matching the dimensions of bare ions. The dissimilarity of behavior of alkylcarbonates and acetonitrile based electrolytes highlights the importance of ion–solvent interactions when searching the optimal porous texture for the electrode material.

1. Introduction

Most industrial electric double layer capacitors (EDLC) are built with porous carbon electrodes, but new devices which combine a battery type electrode and a porous carbon electrode (hybrid supercapacitors or Li-ion capacitors (LIC)) are able to provide higher operating voltages and larger specific energies [1–14]. As the energy stored in an electrochemical capacitor increases, the search of safe and efficient new electrolytes is needed. At this time, the most popular electrolyte is $TEABF_4$ in acetonitrile (ACN), as this its conductivity is very high owing to the low viscosity of ACN and the large dissociation of $TEABF_4$. The main drawback of this electrolyte is a risk of damaging fires which increases with the size of

* Corresponding author. Centre de Recherche sur la Matière Divisée, CNRS – Université, 1b Rue de la Férollerie, 45071 Orléans, France. Tel.: +33 (0) 238257884; fax: +33 (0) 238638103.
E-mail address: raymundo@cnrs-orleans.fr (E. Raymundo-Piñero).

http://dx.doi.org/10.1016/j.jpowsour.2014.04.024
0378-7753/

the electrochemical device owing to the high flammability of ACN. Cyclic alkylcarbonates, like PC, which are far less flammable than ACN, have been proposed as an alternative to ACN as solvent and even mixtures of linear and cyclic carbonates are able to provide a better security [15,16]. When a battery type electrode is used as anode or cathode instead of a porous carbon electrode, a salt containing a lithium cation has to be used, like $LiPF_6$ or LiTFSI, the latest being more stable thermodynamically. Hence different type of electrolytes may be used depending on the type of electrode used (porous carbon electrodes for symmetric EDLCs or a battery type + a porous carbon electrode for hybrid capacitors) and the level of security desired.

Many authors pointed out that the pore size distribution of the active carbon material [16–24] and the electrolyte ions size [27–29] play the most important role on the EDLCs capacitance. Indeed, Chmiola et al. [17] and Raymundo-Piñero et al. [18] showed that the capacitance increases when the pore size distribution is close to the bare electrolyte ions size. Such results are in concordance with previous studies proposing that, when using a standard organic electrolyte i.e. $TEABF_4$ in ACN, ions penetrate in a desolvated state in the carbon pores [28]. Further studies showed that for some moderately activated carbons, matching both the sizes of carbon pores and electrolyte ions does not only enhance the capacitance per unit area, but can also lead to the saturation of the active porosity [19]. As a result, increasing specific capacitance can simultaneously reduce maximum voltage. This feature can be of practical significance as the maximum voltage can be lower than the electrolyte decomposition limits. Therefore, the surface area should be sufficiently large to allow ions electroadsorption over the whole electrolyte voltage window. Relationships between porous texture and capacitance are described in the literature for aqueous or organic electrolytes containing $TEABF_4$ and ionic liquids. However, to our knowledge, the correlation between the capacitance and the carbon textural properties in an electrolyte containing other cations than $TEABF_4$ dissolved in an organic solvent has not been yet fully studied.

When an EDLC or a hybrid supercapacitor is operating, both cations and anions are adsorbed/desorbed at the carbon surface while charging/discharging the supercapacitor and it would be necessary to evaluate the relationship between the carbon pore size and ion size for both of them. Moreover, Morita et al. [25–27] showed that not only the nature of the ionic species, size and chemical properties, but also the solvent or solvent mixture is able to modify the EDLC capacitance owing to ion solvation. The main objective of this work is to investigate the effect of ions size and ions solvation on the electrochemical behavior of symmetrical supercapacitors using as active material a series of porous carbon activated carbons with controlled pore size distribution. The following electrolytes are selected : (I) a 1 mol L^{-1} LiTFSI solution in EC/PC/3DMC (1:1:3 by volume), which has been already identified as an efficient electrolyte for LIC [14], (II) a 1 mol L^{-1} $TEABF_4$ in ACN and (III) a 1 mol L^{-1} LiTFSI in ACN. These electrolytes were prepared for understanding the role of the salt (Li^+ vs TEA^+) and its solvation (alkylcarbonates vs ACN) on the electrochemical performances of porous carbon based electrodes. In this work, the electrochemical behavior of such electrodes will be characterized by cyclic voltammetry, galvanostatic charge/discharge cycles and impedance spectroscopy.

2. Experimental

2.1. Materials

Activated carbons with different textural properties were synthesized by CO_2 activation on precarbonised coconut shells (supplied by PICA) as raw materials. Prior to the activation process the coconut shells were washed with concentrated HF (48%) for 12 h at room temperature, followed by washing with concentrated HCl (32%) for 3 h at 60 °C in order to eliminate the metal impurities. The as-purified precursor was washed with distilled water and then dried at 80 °C in air. Subsequently, the coconut shells (5 g or 10 g) was heated-up to the desired temperature (800 °C or 900 °C) under argon with a heating rate of 5 K min^{-1}. Once the temperature was reached, the Ar flux was switched to CO_2 (3, 4 or 6 L per hour) for several time periods (8–28 h) (see Table 1). After the CO_2 activation phase, the sample was still kept at the same temperature for an hour under Ar before cooling down in the same atmosphere. The as-obtained activated carbons were manually grinded and then sieved with a 40 μm mesh sieve.

All reactants for electrolyte preparation: tetraethylammonium tetrafluoroborate ($TEABF_4$), lithium bis(trifluoromethanesulfonyl) imide (LiTFSI) ethylene carbonate (EC), propylene carbonate (PC), dimethylcarbonate (DMC) and acetonitrile were supplied by Sigma Aldrich and used without further purification. Electrolytes were prepared in an Ar filled glove box and the water content of electrolyte solutions were below 20 ppm as indicated by Karl Fisher titration.

2.2. Chemical and textural characterization

Influence of the activation temperature, activation time and CO_2 flow rate on the characteristics of the activated carbons was studied by several techniques. Material morphology and composition were examined by scanning electron microscopy (Philips model FEI model Quanta 400) equipped with an energy dispersive spectrometer. The textural properties of the carbons were determined from the study of the adsorption isotherms of N_2 at 77 K and CO_2 at 273 K using a Micromeritics ASAP 2020 instrument.

Prior to the analysis, the carbons were out-gassed overnight under vacuum at 300 °C on the degassing port followed by a supplementary out-gassing (4 h) on the analysis port in order to eliminate the backfill gas which could possibly be adsorbed in the micropores during the backfilling step of the analyze tube. This preliminary step appears as of great importance to obtain good quality isotherms in the low pressure range ($P/P_0 < 10^{-6}$) and correct pore size distribution particularly at the microporosity range. The BET surface area (S_{BET}) was calculated from the N_2 adsorption isotherm in the relative pressure range of 0.02–0.3. The microporous (pore diameter < 2 nm) and ultramicroporous (pore diameter < 0.8 nm) volumes were calculated by applying the Dubinin–Raduskevich method respectively to the N_2 ($V_{DR\ N_2}$) and the CO_2 adsorption isotherms ($V_{DR\ CO_2}$) in the range $10^{-4} < P/P_0 < 10^{-2}$. Thus, the volume of mesopores ($2 < d < 50$ nm) can be obtained from the difference of the total pore volume (obtained from the amount of N_2 adsorbed at a relative pressure of 0.95) and $V_{DR\ N_2}$ and the volume of the so-called super-micropores is estimated by the difference $V_{DR\ N_2}$ and $V_{DR\ CO_2}$. The average pore size (L_0) was calculated from the application of the Stoeckli equation to

Table 1
Experimental conditions used for the activation of coconut shell char and burn-off.

Carbon name	Temperature (°C)	Time (h)	Flow rate (l h^{-1})	Burn-off (%)
CA-L	800 °C	28	3	42
CA-I	800 °C	28	4	46
CA-F	800 °C	28	6	53
CA-1	900 °C	8	6	56
CA-2	900 °C	10	6	60
CA-3	900 °C	12	6	66
CA-4	900 °C	14	6	72
CA-5	900 °C	16	6	76

the N_2 adsorption data [29]. The pore size distribution was assessed by Density Functional Theory (DFT) using the model for carbon slit pores on the N_2 adsorption isotherm.

The surface chemistry of the activated carbons was analyzed by thermal programmed desorption (TPD). The total amount of each gas released was computed by time integration of the TPD curves. The active surface area (ASA) was determined by using the method of Walker [30] based on di-oxygen chemisorptions on graphite materials which was further adapted to other type carbon materials [31].

In a first step, the activated carbon surface was cleaned by outgassing at 900 °C for 30 min under high vacuum (10^{-4} Pa). In a second step, the graphite surface was exposed to oxygen (pressure of about 66.5 Pa) at 300 °C for a period of 10 h leading to the formation of surface oxygen complexes. The amount of CO and CO_2 desorbed from the sample resulting from the thermal decomposition of these oxygen complexes is quantified by performing a TPD analysis. Taking into account the number of mole for each gas desorbed and considering the area of an edge carbon site (lying in the (1 0 0) plane) that chemisorbed an oxygen atom as 0.083 nm^2, the surface area occupied by the chemisorbed oxygen (ASA) can be computed.

2.3. Electrochemical characterization

Electrodes were prepared by mixing the carbon materials (85 wt %) with carbon black as conductive additive (5 wt%, C-65 carbon, TIMCAL Co.) and a PTFE binder (10 wt%). The obtained paste was pressed into a 10–15 mg pellets. Capacitors were assembled in a Teflon Swagelok® type system using a glass fiber as separator and titanium plates as current collectors. Electrolytes (I), (II) and (III), described in the introduction section, have been used to fill the Swagelock cells. The gravimetric capacitance expressed in Farads (F) per gram of carbon material was estimated from galvanostatic charge/discharge cycles at increasing current densities of 100, 1000 and 5000 mA g^{-1} using a MPG2 (Biologic, France) multichannel potentiostat. The specific capacitance C (F cm^{-2} S_{DR}) was determined by dividing the gravimetric capacitance (in F g^{-1}), obtained in the 2.5 V voltage range, by the DR specific surface area ($S_{DR\ N_2}$, in cm^2 g^{-1}).

Impedance spectroscopy measurements were performed on Swagelock cells at different state of charge by applying an ac signal with an amplitude of 20 mV (VMP2, Biologic, France). Data were collected in the range of 10 000 Hz–0.001 Hz.

2.4. Theoretical approach for ion size, ion volume, polarizing power and polarizability

The same methodology as already presented by Ab Manan et al., [32] was used to optimize each 3D structure (Gaussian version 03-D1, DFT-B3LYP-DGTZVP) [33] and to generate then, from this resultant optimized structure, its COSMO file (TURBOMOLE, BP-DFT-Ahlrichs-TZVP) [34]. The COSMO volume of the studied ions and solvent molecules were obtained by using the COSMOthermX software (version 2.1, release 01.06) [35] based on the COSMO-RS (Conductor-like Screening Model for Real Solvents) model [36]. The calculation method used for the polarizing power and the polarizability was based on the work of Miller and Savchik [37].

3. Results and discussion

3.1. Physico-chemical characterization of the raw material

Pre-carbonized coconut shells were used as raw material to prepare the activated carbons. They display a granular morphology with an average particle size of about 1–1.5 mm as shown by SEM images (Fig. 1). At a higher magnification scale, a dense morphology is observed with holes between 0.5 and 10 μm in size. The material contains besides C and O, metals (K, Ca, Si, Na, Al) and Cl as revealed by EDX analysis. The concentration of these impurities is less than 1.5 wt% and after washing with HF and HCl, such amount is reduced to 0.12 wt%. The specific surface area of the carbonized material (S_{BET}) is around 50 m^2 g^{-1}.

3.2. Physico-chemical characterization of the activated carbons

The experimental conditions used to prepare the activated carbons are summarized in Table 1.

The textural characteristics of the carbon materials were determined by N_2 and CO_2 adsorption. The N_2 adsorption/desorption isotherms (Fig. 2) are of type I according to the IUPAC classification [38], which are specific to microporous materials. A sharp increase of N_2 uptake at very low relative pressures and an almost horizontal plateau without any adsorption/desorption hysteresis characterize the isotherms of all materials under study. The adsorption isotherm of the raw material, which is a nonporous material, has been omitted for clarity in Fig. 2. The values of the textural characteristics derived from the N_2 and CO_2 isotherms are gathered in Table 2. The as-prepared carbon materials display surface area between 800 m^2 g^{-1} and 1934 m^2 g^{-1} (Table 2). They are mainly microporous with a fraction of ultramicropores. As underlined in Table 2, the porosity can be tailored by the control of the flow rate, temperature and activation time. At a given temperature (800 °C) and activation time (28 h), the specific surface area and the microporous volume increase with the flow rate whereas the ultramicroporous volume remains almost constant. The same trend is observed at 900 °C by changing the activation time at a constant flow rate. It also appears in Table 2 that the

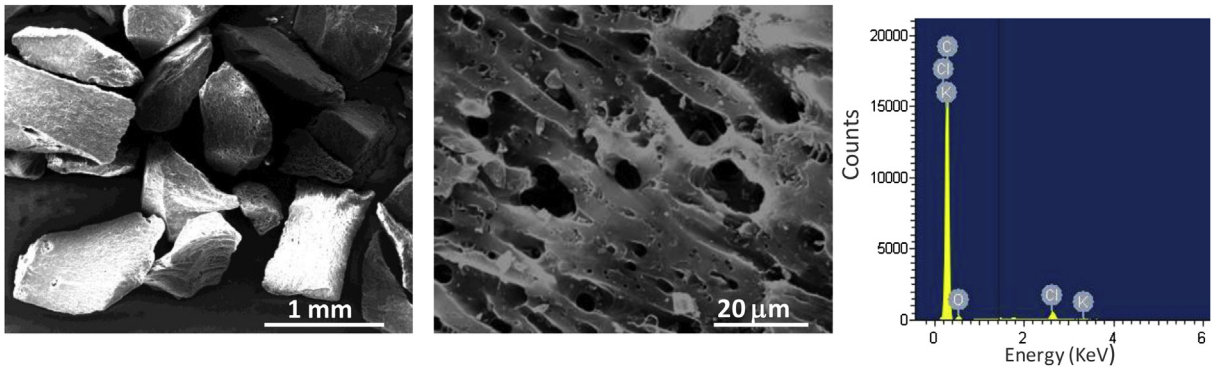

Fig. 1. SEM pictures and EDX spectra of washed coconut shells.

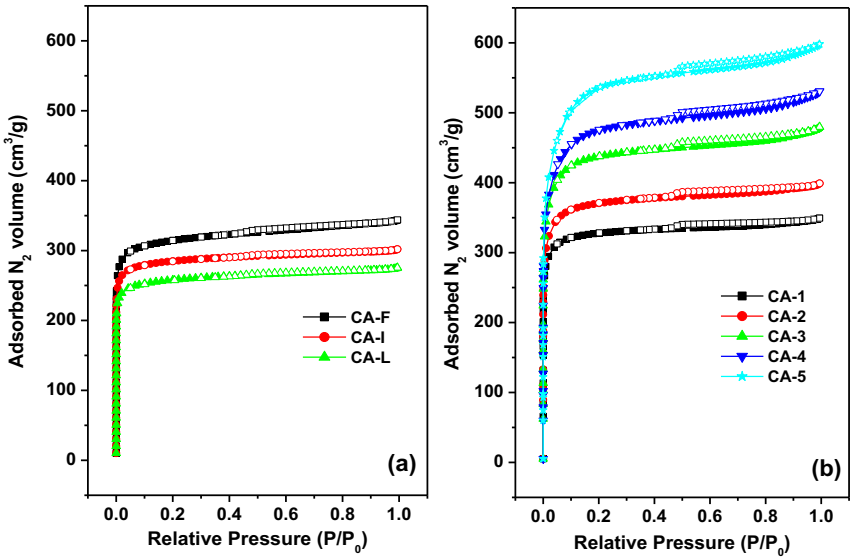

Fig. 2. Nitrogen adsorption/desorption isotherms made at 77 K on different activated carbons obtained at (a) 800 °C and (b) 900 °C.

mesoporous volume increases only for activation time at 900 °C longer than 12 h.

For all synthesized samples, an almost linear relationship is found, between the microporous volume and the burn-off (Fig. 3), confirming the highly selective nature of the CO_2 activation regarding the microporosity development [39].

Fig. 4 shows the DFT pore size distribution of the activated carbons. For the carbons prepared at 800 °C, the average pore size (L_0) slightly increases with the flow rate and very small micropores with sizes centered around 0.5 nm are predominantly formed (Fig. 4a). For materials prepared at 900 °C, the average pore size increases with the activation time and small mesopores ($d > 2$ nm) appear. In addition, the average pore size increases linearly with the burn-off as pointed out by Fig. 3.

The surface chemistry and the active surface area of the carbons were determined by TPD coupled with mass spectrometry and oxygen chemisorption, respectively.

The thermal decomposition of the surface oxygenated groups leads to the formation of gases such as CO and CO_2. The release temperature of these gases gives indication of their chemical nature. For all the porous carbons, we observed a considerable CO desorption peak at high temperatures (700–900 °C), indicating the presence of oxygenated groups such as ethers and quinones [40–42]. The CO_2 evolution is significantly lower and is mainly located between 50 and 300 °C suggesting the presence of carboxyl groups [40,41]. Furthermore, a certain amount of hydrogen is desorbed from the materials at high temperature (~900 °C) suggesting the cleavage of C–H bonds. The integration of desorption peaks allows to quantify the amounts of the oxygenated groups released from the carbon surface (Table 3). Results reported in Table 3 show that all activated carbons possess a similar amount of oxygen functionalities desorbing as CO or CO_2.

As shown in a previous paper, the surface defect concentration (ASA) plays also an important role in regard to the surface/electrolyte interaction [43]. The ASA values of the activated carbons are listed in Table 3 and it can be noticed that an almost constant value is obtained whatever the preparation conditions of the carbons. Moreover, the ASA values reported to the carbon specific surface area are quite low (see Table 3).

Therefore, we were able to prepare a series of activated carbons exhibiting different textural characteristics without changing their surface chemistry or/and active surface area. This allows us to focus our study only on the effect of the textural properties on the electrochemical performance.

In summary, by varying the activation conditions, it was possible to obtain a series of porous carbons with specific surface areas ranging from 800 to 1900 $m^2\ g^{-1}$ facing with a gradual increase on their average pore size from 0.72 nm up to 1.48 nm. Such a series

Table 2
Textural properties of the activated carbons.

Carbon name	S_{BET} ($m^2\ g^{-1}$)	$S_{DR\ N_2}$ ($m^2\ g^{-1}$)	$V_{DR\ N_2}$ ($cm^3\ g^{-1}$)	V_{meso} ($cm^3\ g^{-1}$)	$V_{DR\ CO_2}$ ($cm^3\ g^{-1}$)	L_0 (nm)
CA-L	803	1098	0.39	0.03	0.27	0.72
CA-I	886	1239	0.44	0.02	0.28	0.76
CA-F	981	1351	0.48	0.05	0.31	0.86
CA-1	1021	1408	0.50	0.03	0.34	0.95
CA-2	1156	1549	0.55	0.06	0.35	1.15
CA-3	1328	1774	0.63	0.10	0.34	1.28
CA-4	1746	2140	0.76	0.25	0.31	1.30
CA-5	1934	2197	0.78	0.34	0.31	1.48

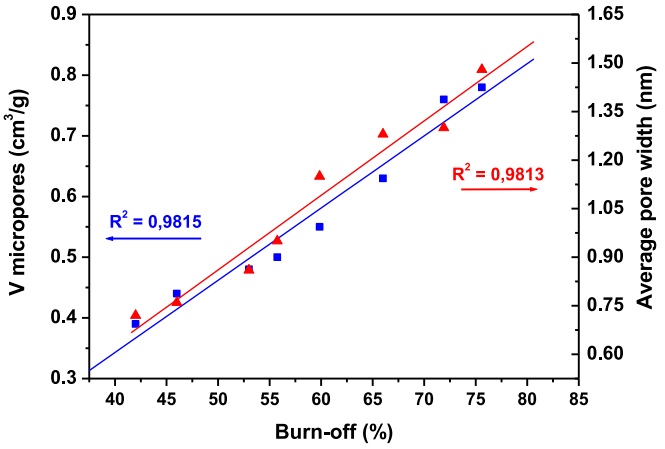

Fig. 3. Relationship between the burn-off and the microporous volume and the average pore size for carbons activated at two different temperatures (a) 800 °C and (b) 900 °C.

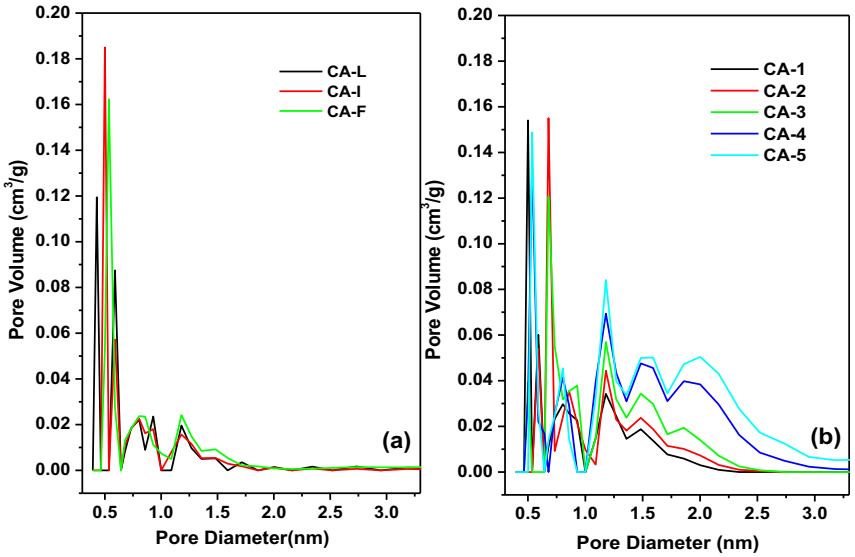

Fig. 4. DFT pore size distribution for different activated carbons obtained at (a) 800 °C and (b) 900 °C.

will be of a great help for understanding the role of the porous texture on the electrochemical performances of supercapacitors operating with different electrolytes.

3.3. Electrochemical performance

3.3.1. Influence of the electrolyte composition on the electrochemical performance

The electrochemical performances of activated carbons were first analyzed by using a two-electrodes cell to which galvanostatic charge–discharge cycles were applied at a current density of 100 mA g^{-1}. The specific capacitance of the activated carbons, determined in the electrolytes (I), (II) and (III) is plotted versus they average pore size L_0 in Fig. 5. The trend obtained for the LIC electrolyte (I) containing the alkylcarbonate mixture is different from the others. As a matter of fact, using ACN as solvent, the typical trend for which the specific capacitance increases when decreasing the average pore sizes to values smaller than 1.0 nm is obtained, while it remains constant for wider pore sizes. As it has been reported in the literature, such behavior is related to the increase of the efficiency of the double layer formation when the size of the pores is close to the size of the ions [17,18,21]. As for $TEABF_4$ in ACN, it has been demonstrated that the ions penetrate the porosity partially or totally desolvated [17,18,21,28], the pores fitting the size of the TEA^+ ion (~0.75 nm) which is larger than the BF_4^- (~0.50 nm) are smaller than 1.0 nm (refer to Table 4). Nevertheless, Fig. 5 shows that the supercapacitors built with the carbon having the smaller surface area (i.e. CA-L) present a specific capacitance smaller than expected by considering the carbon average pore size. Such behavior is related to another phenomenon identified as a surface saturation in this electrolyte [19] as the voltammograms, presented in Fig. 6II, exhibit a decrease in specific current density and hence, charge, for the CA-L capacitor at voltages higher than 1.5 V. That means that there is not enough surface available at the CA-L carbon interface for accommodating all TEA^+ ions while charging the supercapacitor up to 2.5 V. However after slightly increasing the surface area of the electrode material i.e. using CA-I, the saturation effect becomes almost negligible as the surface is high enough for accepting charges up to a cell voltage of 2.5 V.

The surface saturation effect depends on the size of the electrolyte ions as shown when using LiTFSI in ACN (electrolyte III). The voltammograms presented in Fig. 6III do not exhibit any saturation effect, even for the carbon having the smallest surface area and pore size. Table 4 shows that unsolvated Li^+ or $TFSI^-$ ions present at least one of their dimensions which is considerably smaller than the TEA^+ radius i.e. the ions with the largest dimensions in $TEABF_4$.

Table 3
Quantities of oxygenated groups desorbed from the surface of activated carbons as determined by integration of the TPD-MS peaks and the active surface area.

Carbon	CO, mmol g^{-1}	CO_2, mmol g^{-1}	ASA, (m^2 g^{-1})	ASA/$S_{DR\ N_2}$	wt% O
CA-1	0.63	0.17	45.1	0.032	1.6
CA-2	0.69	0.19	47.7	0.031	1.7
CA-3	0.79	0.23	42.7	0.024	2.0
CA-4	0.76	0.27	48.3	0.023	2.1
CA-5	0.68	0.19	48.1	0.022	1.7
CA-F	0.81	0.18	n.a.	n.a.	1.9

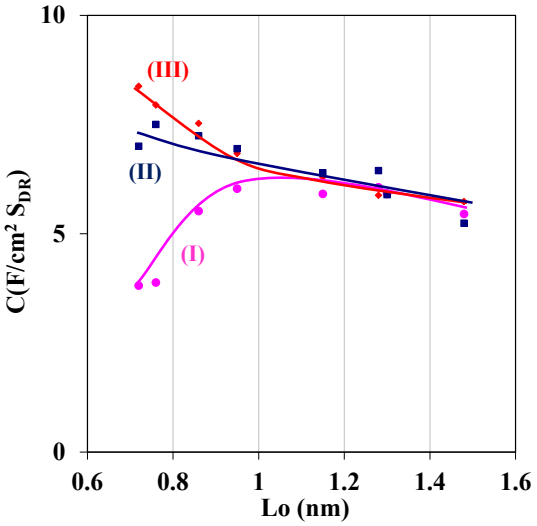

Fig. 5. Relation between the specific capacitance normalized by DR SSA and the pore size in 1 mol L^{-1} LiTFSI in EC/PC/3DMC, 1 mol L^{-1} (I) 1 mol L^{-1} $TEABF_4$ in ACN (II) 1 mol L^{-1} LiTFSI in ACN (III) for the complete series of activated carbon at 100 mA g^{-1}.

Table 4
Structure, size and COSMO volume of solvent molecules and ions under study evaluated by Gaussian interface. Polarizing power of ions ($|Z|/r_{ion}$), polarizability (α) and dipole moment (μ) of solvent molecules.

Molecule/ion	Structure **Structure** -0.03 -0.02 -0.01 0.00 0.01 0.02 0.03 Polarisation Charge Density σ	Size min/max length (nm)	COSMO volume (Å^3)	$\|Z\|/r_{ion}$ (Å^{-1})	α (cm^3)	μ (D)
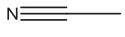 acetonitrile **ACN**	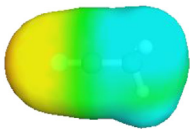	0.40/0.58	63.7	/	4.44	3.92
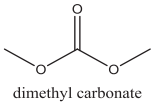 dimethyl carbonate **DMC**	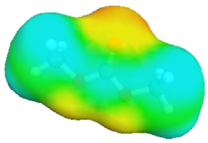	0.41/0.87	108.3	/	7.58	0.91
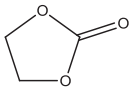 1,3-dioxolan-2-one **EC**	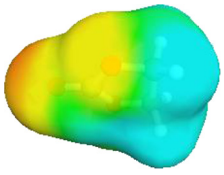	0.49/0.67	94.2	/	6.87	5.35
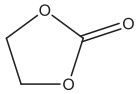 1,3-dioxolan-2-one **PC**	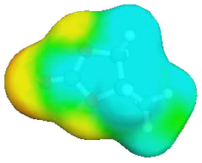	0.52/0.77	116.2	/	8.71	4.94
Li^+		0.13/0.13	16.2	1.54	/	/
Et_4N^+	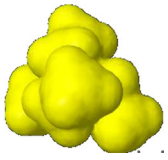	0.75/0.85	202.8	0.13	/	/
BF_4^-	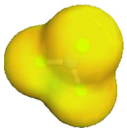	0.50/0.51	72.8	0.20	/	/
$TFSI^-$	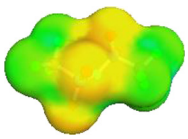	0.37/0.75	219.7	0.18	/	/

Hence, the accessible surface area of the electrode material will be higher for LiTFSI than for $TEABF_4$ based electrolytes, being enough to accommodate all the charges even for the lower surface area carbon material and the highest state of charge. As a consequence, the specific capacitance in the LiTFSI/ACN electrolyte, reported in Fig. 5, follows the expected ascendant trend when decreasing the average pore size.

Therefore, as the same trend is not observed for the alkylcarbonate based electrolyte containing the same salt, we have to take into account the possible effect of the solvation. In the case of the alkylcarbonates mixture, EC and to a lower extent PC, which has the strongest dipole moment (see Table 4), are the predominant molecules in the solvation sphere of the Li^+ cation [44,45]. The solvation of an ion by solvent molecules is the result of ion-dipole and

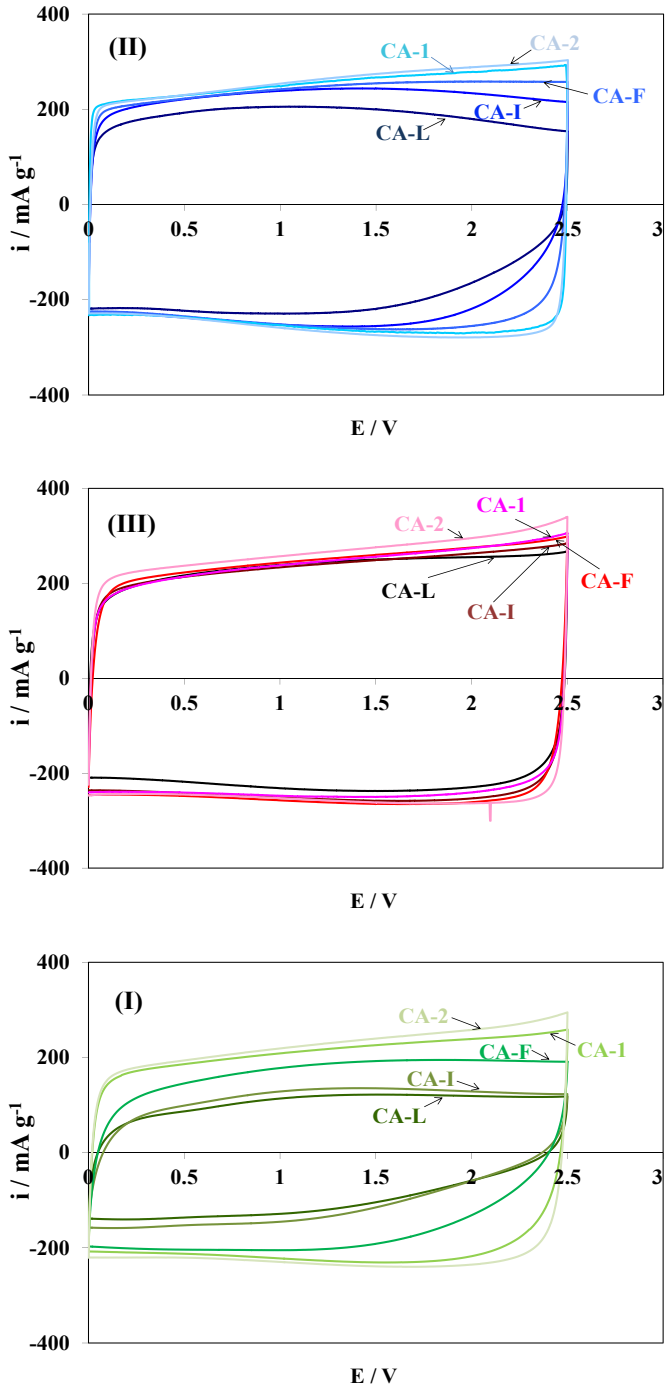

Fig. 6. Cyclic voltammogramms at a sweep rate of 5 mV s^{-1} of the supercapacitors using a two-electrode cell in 1 mol L^{-1} $TEABF_4$ in ACN (II), 1 mol L^{-1} LiTFSI in ACN (III) and 1 mol L^{-1} LiTFSI in EC/PC/3DMC (I) at 100 mA g^{-1}.

ion-induced dipole interaction which can be evaluated by mean of the ion polarizing power, the solvent dipole momentum and polarizability. The ions polarizing power is its ability to distort the electronic cloud of other molecules and the polarizability is the tendency of the electronic cloud of a molecule to be distorted by neighboring ions. The polarizing power ($|Z|/r_{ion}$), the polarizability (α) and the dipole moment (μ) of ions and solvent molecules under study [46,47] are reported in Table 4.

Therefore, a small highly charged cation like Li^+ with a high polarizing power shell distort the electronic cloud of the solvent molecules (higher in size) in a manner that it increases the electron density between the Li^+ ion and the solvent molecule depending on its polarizability. This effect is even reinforced if the molecule is strongly polar like EC or PC. Polarization and ion-dipole interaction will induce a covalent like Li–(Solvent) binding making it difficult to strip molecules from the solvation shell. Such distortion of the solvent electron cloud will be very important when using highly polarizable solvents as EC or PC but less for more slightly polarizable molecule as ACN. As a consequence, in the presence of the high electrical field which occurs at the vicinity of the electrode surface when the supercapacitor is charged, Li^+ ions will more easily loss their solvation shell if the solvent is ACN instead of alkylcarbonates like EC or PC. Considering the standard electrolyte ($TEABF_4$ in ACN), which contains TEA^+ and BF_4^- of low polarizing power (0.125 and 0.20 $Å^{-1}$, respectively), in the weakly polarizable ACN, it is not surprising that these ions can easily loss their solvation shell under the same electrical field. The same is valid for LiTFSI in ACN as the polarizing power of the TFSI anion is only 0.18 and as ACN exhibit a much lower polarizability and dipole moment than cyclic alkylcarbonates. Therefore, for $TEABF_4$ or LiTFSI salts in ACN, one can consider the size of the bare ions for assessing the accessible electrode material pore size. In particular, for $TEABF_4$ in ACN a pore size of around 0.75 nm is enough for the ions to penetrate and for the LiTFSI in ACN all the porosity can be invaded as pore diameters of only 0.37 nm are enough for the ions to enter. However, when using LiTFSI in the alkylcarbonates mixture the solvation shell must be accounted for determining the size of the species penetrating the porosity. So, as Li-ions with a first solvation sphere constituted mainly by EC molecules will have a diameter of around 1.11 nm ($Ø = 2 \times 0.49$ (EC) + 0.13 (Li^+)), only the pores having a diameter wider than such dimension will be used for forming the double layer. Therefore, this is the reason why for electrolyte using alkylcarbonates based electrolyte, the specific capacitance is quite low for materials having small average pore sizes with almost no pores wider than 1.0 nm (CA-L, CA-I and CA-F materials as shown in the PSD presented in Fig. 3) and increases when the average pore sizes of the electrode materials increase owing to the presence of pores wider than 1.0 nm (from CA-1 carbon material as shown in the PSD presented in Fig. 3) where solvated ions can penetrate.

3.3.2. *Influence of the current density on the electrochemical behavior*

The differences in solvation together with the differences in conductivity of the electrolytes will have an additional important impact on the internal resistance of the supercapacitor and therefore, on the power density. Table 5 presents the conductivity values of the three electrolytes used in the present study and the electrical series resistances (ESR) obtained from impedance spectroscopy analysis performed on supercapacitors having as electrode material the porous carbon with the smaller average pore size i.e. CA-L ($L_0 = 0.72$ nm), and a porous carbon having a wider average pore size i.e. CA-2 ($L_0 = 1.15$ nm). The ESR is related to the sum of the electrode materials, interfaces and electrolyte resistances. Table 5 shows that the ESR values are generally higher for the CA-2

Table 5
Comparison of CA-L and CA-2 Electrical Series Resistances (ESR) with the bulk conductivity of the three electrolytes: (I) 1 mol L^{-1} $TEABF_4$ in CAN, (II) 1 mol L^{-1} LiTFSI in ACN, and (III) 2 mol L^{-1} LiTFSI in EC/PC/3DMC.

Electrolyte	Electrolyte conductivity (S cm^{-1})	CA-L cell ESR (Ω)	CA-2 cell ESR (Ω)
$TEABF_4$/ACN	60	1.9	2.4
LiTFSI/ACN	29	1.3	2.4
LiTFSI/(EC/PC/3DMC)	8	9.0	4.7

supercapacitor than for the CA-L, reflecting the decrease in conductivity of the carbon material when developing porosity. Comparing supercapacitors build with the same electrode material but different electrolytes, the highest ESR is obtained when using the less bulk conductive electrolyte i.e. LiTFSI in EC/PC/3DMC.

Nevertheless, the higher influence of the electrode–electrolyte couple on the system resistance is found when measuring the electrical distributed resistance (EDR). The EDR is mainly related to the diffusion of ions into the charging storage material i.e. into the pores in the case of porous carbons. The dimensions of the species penetrating the porosity will have the key role in the case of the CA-L electrode active material owing to its narrow pore size. In this sense, Fig. 7 shows that for CA-L based supercapacitor, the EDR at any cell voltage is similar when using electrolytes containing ACN as solvent as the ions penetrate the porosity at the desolvated state and any steric effect applies. However, for the electrolyte using the alkylcarbonate mixture, EDR values are markedly higher than for the ACN indicating the difficulty of ions for diffusing into the accessible porosity when accompanied by their solvation shell. Fig. 7 shows that such difficulty will increase when raising the cell voltage. The reason of such behavior resides in the fact that the CA-L carbon material possesses a small accessible surface area for the solvated ions which will be rapidly occupied at a low state-of-charge and a further deformation or partial stripping of the solvation cell will be needed to have access into smaller pores for continuously charges storing [48]. In contrast, for a supercapacitor using carbon electrode material such as CA-2, with average pore sizes allowing the penetration of alkylcarbonate solvated ions, the EDR drastically decreases to values closer to those obtained for the supercapacitors built using ACN based electrolytes and same active material. Nevertheless, EDR values in the alkylcarbonate electrolyte are still higher than in ACN because of the additional kinetic constraint for ions to diffuse inside the porosity together with solvent molecules.

In order to appreciate the effect of the above-discussed resistances on the electrochemical behavior of the supercapacitor at high current regime, the capacitance retention vs the applied current density has been reported in Fig. 8 for all supercapacitors built with porous carbons and the three different electrolytes. It can be noticed that the capacitance behavior depends on both the electrolyte salt and the solvent. Fig. 8II shows that for the standard

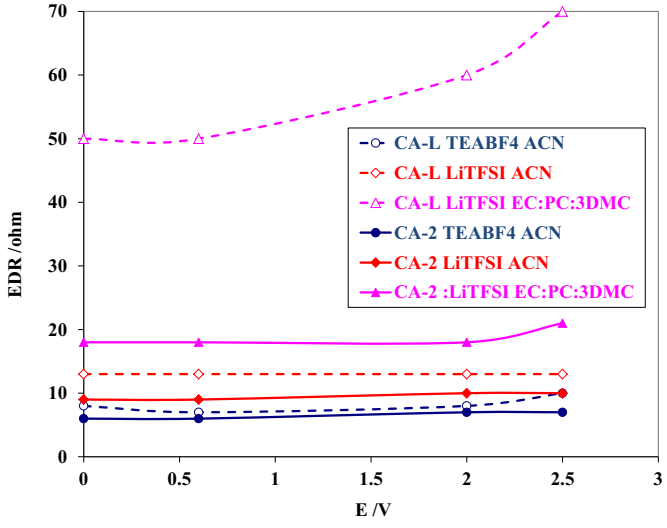

Fig. 7. Evolution of the Electrical Diffusion Resistance (EDR) as a function of cell voltage in 1 mol L^{-1} $TEABF_4$ in ACN, 1 mol L^{-1} LiTFSI in ACN and 1 mol L^{-1} LiTFSI in EC/PC/3DMC for CA-L and CA-2.

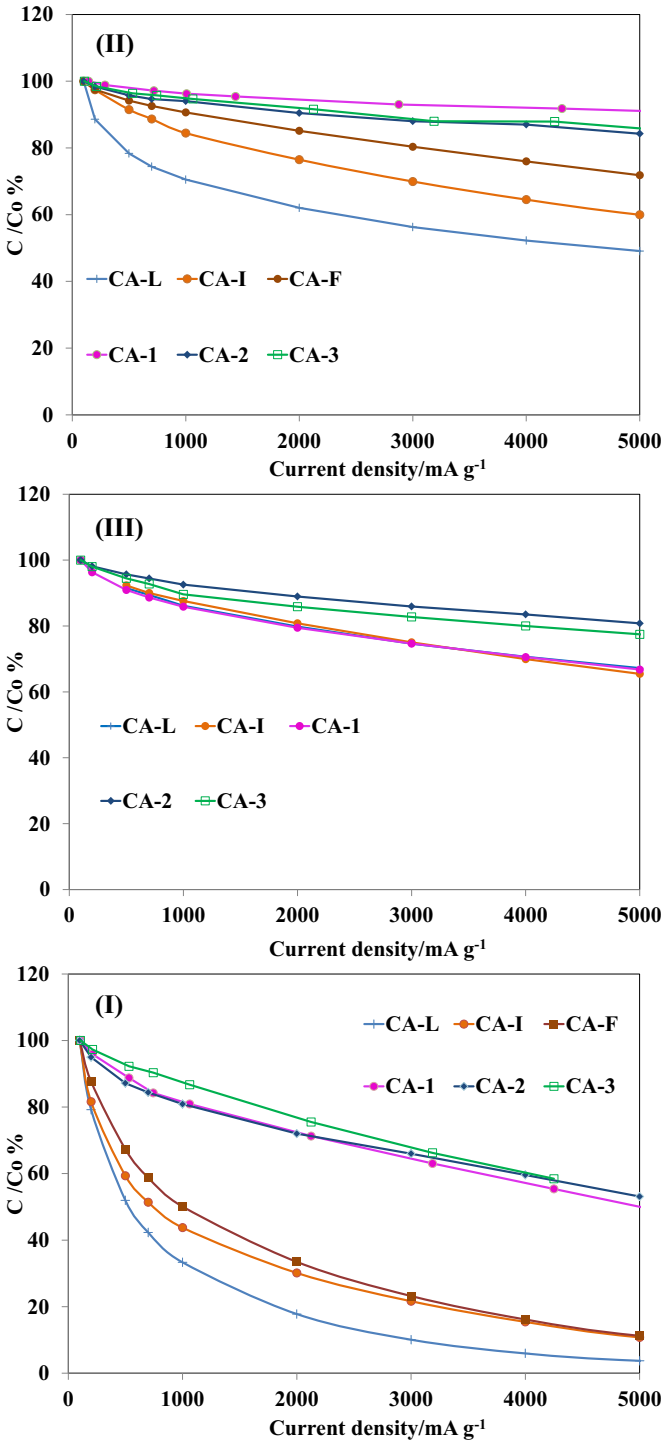

Fig. 8. Evolution of the capacitance retention as a function of the applied current density for the supercapacitors built with the series of porous carbons in the three different electrolytes: 1 mol L^{-1} $TEABF_4$ in ACN (II), 1 mol L^{-1} LiTFSI in ACN (III) and 1 mol L^{-1} LiTFSI in EC/PC/3DMC (I).

organic electrolyte i.e. $TEABF_4$ in ACN, the loss of capacitance through increasing the current density is more pronounced when the carbon material is smaller in pore size. That means that for electrode materials having an average pore size matching the dimensions of the TEA^+ ions, the diffusion of such ions becomes difficult when increasing the current density. Such kinetic limitations are smaller when increasing the pore size of the carbon

material (see Fig. 8II), indicating that probably at large current densities ions are not able to completely loss their solvation sphere and steric limitations will apply when the size of the pores will be close to the dimensions of the bare ions. As a consequence, the advantages in term of capacitance of a pore size matching the ions dimensions are lost at high current densities and we cannot find anymore the ascendant trend of the specific capacitance when decreasing the pore size (see Fig. 9 presenting the specific capacitances obtained at current densities of 1000 mA g^{-1} (a) and 5000 mA g^{-1} (b)). Such affirmation can be supported by the results presented in Fig. 8III showing that for an electrolyte containing smaller ions but using the same solvent i.e. LiTFSI in ACN, there is no effect of the pore size on the capacitance retention at high current densities. Indeed, even for supercapacitors built with the carbon material having the smaller pore size, the capacitance retention at high currents is the same than for those including materials having wider pores. Hence when using electrolyte designed for LIC application i.e. LiTFSI in EC/PD/3DMC, once the pore size of the electrode material is large enough to accommodate the solvated ions, no effect of the pore size on the capacitance retention at high current densities can be observed (see Fig. 8I).

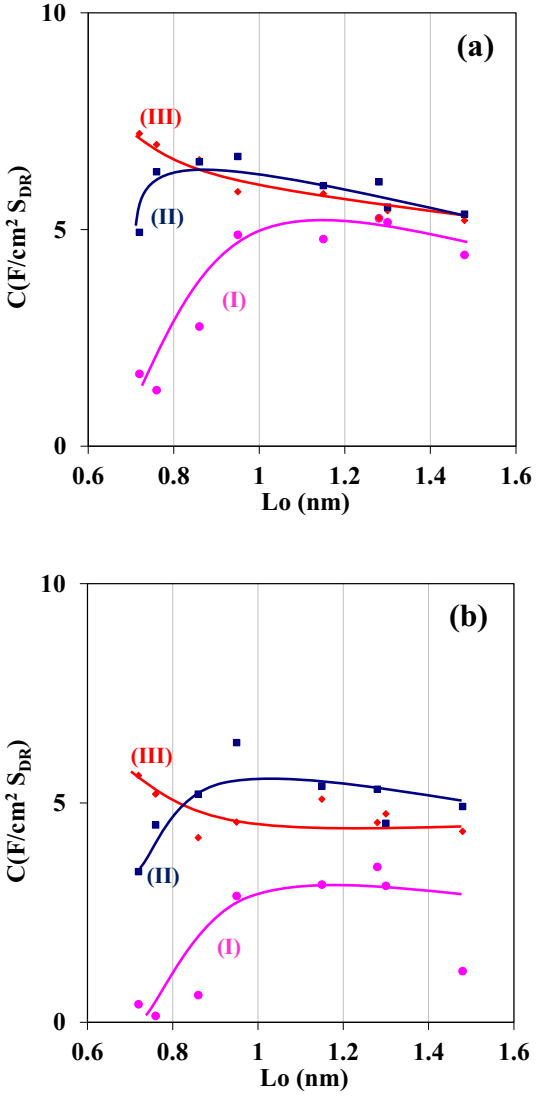

Fig. 9. Specific capacitance normalized by S_{DR} vs the average pore size in 1 mol L^{-1} LiTFSI in EC/PC/3DMC (I), 1 mol L^{-1} LiTFSI in ACN (II) and 1 mol L^{-1} $TEABF_4$ in ACN (III) for the complete series of activated carbon at 1000 mA g^{-1} (a) and 5000 mA g^{-1} (b).

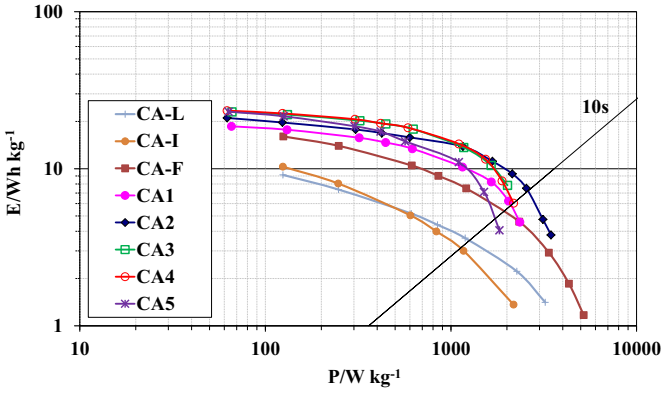

Fig. 10. Ragone plots for the supercapacitors using the series of porous carbons in 2 mol L^{-1} LiTFSI EC/PC/3DMC.

Therefore, at the difference to standard organic electrolyte, LiTFSI based electrolytes follow the relationship established between the specific capacitance and the pore size whatever the applied current density. Fig. 9 shows that for the two electrolytes containing LiTFSI we can just observe a shift of the curves in the *Y*-axis direction to smaller specific capacitance values when increasing the current density (compare Figs. 5 and 9).

Nevertheless, as the LIC electrolyte presents the most important capacitance loss through increasing the current density (see Fig. 9), it would be necessary to assess the performances in terms of power densities when operating in such as electrolyte. At that moment it should be pointed out that a supercapacitor is basically a power device and even if the energy density can be markedly enhanced by using a LIC configuration [1–14], the power density must be enough high to keep the advantage of such a system over a battery.

In this sense, Fig. 10 depicts the Ragone plots for the supercapacitors using the series of porous carbons in LiTFSI EC/PC/3DMC as electrolyte. It can be noticed that at low power densities, the maximum energy, which can be extracted, is similar for the supercapacitors built with the activated carbons having pore sizes wide enough for the solvated electrolyte ions to penetrate. However, at higher regimes the extractable energy for a given power depends on the porous material used. In particular, Fig. 11 shows

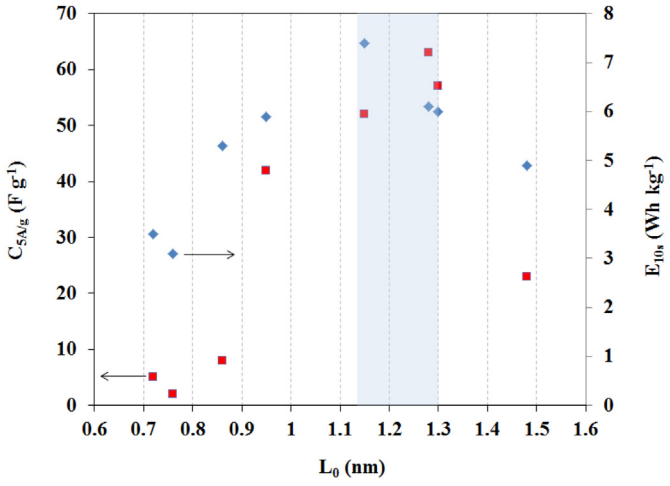

Fig. 11. Evolution of the energy available (blue) and the capacitance at 5 A g^{-1} (red) for a discharge time of 10 s (obtained from the Ragone plot) as a function of the average pore size of the electrodes materials. (For interpretation of the references to color in this figure legend, the reader is referred to the web version of this article.)

that after representing the energy available for a discharge time of 10 s (obtained from the Ragone plot) vs the average pore size of the electrodes materials, there is an optimum size for harvesting the higher power density. Actually, such optimum pore size answer to the matching of several requirements: i) the pore diameters are enough large for allowing the charges to penetrate at a high charging regime. Fig. 11 shows that the materials having pore sizes smaller than 0.9 nm does not allow the diffusion of any solvated ions inside of the porosity and the capacitance at a high current density is negligible; ii) the pore diameters are not too large for decreasing the efficiency of the double layer formation (in reason of the inverse relationship between the last and the average distance from the charged ion centre to the charged pore wall). In this sense, Fig. 11 confirms that at high regimes, the capacitance decreases when the pore sizes are wider than 1.3 nm; iii) the development of porosity should not be too extensive in order to not increase the resistance of the carbon material which will have a negative impact on the power density.

In summary, for a supercapacitor operating in an electrolyte such as LiTFSI in an alkylcarbonate mixture, the optimum pore size of the electrode material giving the best compromise between energy density and power density, must be comprised between 1.1 and 1.3 nm.

4. Conclusions

A series of porous carbons with surface areas ranging from 800 to 1900 $m^2 g^{-1}$ and tuneable average pore sizes varying from 0.7 to 1.4 nm was prepared by CO_2 activation of a pre-carbonized coconut shell precursor by controlling the reaction conditions. Such materials have been shown as very useful for assessing the optimum porous texture needed for carbon electrode materials to efficiently operate in electrolytes designed for symmetrical supercapacitors and newly developed systems as Li ion capacitors (LIC).

It has been shown that for porous carbon based electrodes using Li^+ containing electrolytes such as LiTFSI in EC/PC/DMC, the relationship between the carbon electrode material average pore size and the specific capacitance does not follow the same trend than in the standard organic electrolyte i.e. $TEABF_4$ in ACN. For the last, there is a continuous increase of the specific capacitance when decreasing the average pore size from 1.0 nm down to 0.75 nm and the same trend has been found when using LiTFSI in ACN. On the contrary, for LiTFSI in EC/PC/3DMC, the specific capacitance is low for carbon materials having pore sizes in the range 0.7–0.8 nm (for which a maximum is reached for other electrolytes as $TEABF_4$ in ACN) but increases when widening the average pore size.

The dissimilarity of behavior of ACN and alkylcarbonates based electrolytes highlights the importance of ion–solvent interactions when searching an optimal porous texture for the electrode material: whereas in ACN electrolytes, ions are easily desolvated and can penetrate small pores matching the dimensions of bare ions, in alkylcarbonate based electrolytes ions do not completely loss their solvation shell and wider pores are needed for electroadsorption. The main reason is that solvents like EC which are more polarizable than ACN and exhibit a larger dipole moment, will bind more strongly to small ions as Li^+. The strong Li^+-EC solvation will in turn makes it difficult the stripping of the solvation shell by the electric field which exists at the electrode surface.

Furthermore, the presence of the solvation shell has an important impact on the optimum pore size required to deliver the maximum power density. As the ions are accompanied by some solvent molecules, a pore size large enough for allowing the free diffusion of charges at high current densities is required, but if the pore size is too large the formation of the double layer will be affected and the capacity will decrease.

The average pore size giving the best compromise for obtaining the highest energy density while keeping the power density at a high level lays in the range 1.1 nm–1.3 nm. It is important to note that this pore size is different from that reported in the literature for supercapacitors working in conventional electrolytes such as $TEABF_4$ in acetonitrile. Hence, this finding is of great importance for the prospective industrial systems in need of optimization of carbon electrode materials to be used in electrolytes containing highly polarizing ion such as Li^+ in highly polar solvents such as alkylcarbonates or lactones.

Acknowledgments

This work was financially supported by the French National Agency for Research (ANR): Stock-E project HIPASCAP (ANR-09-STOCK-E-04).

References

[1] N. Ando, S. Taguchi, Y. Hato, Organic Electrolyte Capacitor, EP1400996A1, 2002.
[2] S. Tasaki, N. Ando, M. Nagai, A. Shirakami, K. Matsui, Y. Hato, Lithium Ion Capacitor, WO 2006/112068, 2006.
[3] N. Ando, K. Kojima, S. Tasaki, H. Taguchi, T. Fujii, Y. Hato, C. Marumo, Organic Electrolyte Capacitor, US2007/0002524A1, 2007.
[4] H. Tanizaki, N. Ando, Y. Hato, Lithium-Ion Capacitor, EP1914764A1, 2007.
[5] T. Aida, K. Yamada, M. Morita, Electrochem. Solid-State Lett. 9 (2006) A534–A536.
[6] T. Aida, I. Murayama, K. Yamada, M. Morita, J. Electrochem. Soc. 154 (2007) A798–A804.
[7] T. Aida, I. Murayama, K. Yamada, M. Morita, Electrochem. Solid-State Lett. 10 (2007) A93–A96.
[8] G.G. Amatucci, F. Badway, A. Du Pasquier, T. Zheng, J. Electrochem. Soc. 148 (2001) A930–A939.
[9] A. Du Pasquier, I. Plitz, J. Gural, S. Menocal, G.G. Amatucci, J. Power Sources 113 (2003) 62–71.
[10] M. Schroeder, M. Winter, S. Passerini, A. Balducci, J. Electrochem. Soc. 159 (2012) A1240–A1245.
[11] S.R. Sivakkumar, A.G. Pandolfo, Electrochim. Acta 65 (2012) 280–287.
[12] M. Schroeder, M. Winter, S. Passerini, A. Balducci, J. Power Sources 238 (2013) 388–394.
[13] V. Khomenko, E. Raymundo-Piñero, F. Béguin, J. Power Sources 177 (2008) 643–651.
[14] C. Decaux, G. Lota, E. Raymundo-Piñero, E. Frackowiak, F. Béguin, Electrochim. Acta 86 (2012) 282–286.
[15] P. Kurzweil, in: J. Garche (Ed.), Encyclopedia of Electrochemical Power Sources, Elsevier B.V., 2009, pp. 607–633.
[16] P. Liu, M. Verbrugge, S. Soukiazian, J. Power Sources 156 (2006) 712–718.
[17] J. Chmiola, G. Yushin, Y. Gogotsi, C. Portet, P. Simon, P.L. Taberna, Science 313 (2006) 1760–1763.
[18] E. Raymundo-Piñero, K. Kierzek, J. Machnikowski, F. Béguin, Carbon 44 (2006) 2498–2507.
[19] R. Mysyk, E. Raymundo-Piñero, J. Pernak, F. Béguin, J. Phys. Chem. C 113 (2009) 13443–13449.
[20] D. Lozano-Castelló, D. Cazorla-Amorós, A. Linares-Solano, S. Shiraishi, H. Kurihara, A. Oya, Carbon 41 (2003) 1765–1775.
[21] P. Simon, Y. Gogotsi, Nat. Mater. 7 (2008) 845–854.
[22] G.Z. Gong, Q. Xie, Y.F. Zheng, S.F. Ye, Y.F. Chen, New Carbon Mater. 24 (2009) 141–146.
[23] S. Vaquero, R. Díaz, M. Anderson, J. Palma, R. Marcilla, Electrochim. Acta 86 (2012) 241–247.
[24] C.X. Zhang, R. Zhang, B.L. Xing, G. Cheng, Y.B. Xie, W.M. Qiao, L. Zhan, X.Y. Liang, L.C. Ling, New Carbon Mater. 25 (2010) 129–133.
[25] T. Ohta, I.T. Kim, M. Egashira, N. Yoshimoto, M. Morita, J. Power Sources 198 (2012) 408–415.
[26] I.-T. Kim, M. Egashira, N. Yoshimoto, M. Morita, Electrochim. Acta 55 (2010) 6632–6638.
[27] I.-T. Kim, M. Egashira, N. Yoshimoto, M. Morita, Electrochim. Acta 56 (2011) 7319–7326.
[28] C. Vix-Guterl, E. Frackowiak, K. Jurewicz, M. Friebe, J. Parmentier, F. Béguin, Carbon 43 (2005) 1293–1302.
[29] F. Stoeckli, E. Daguerre, A. Guillot, Carbon 37 (1999) 2075–2077.
[30] N.R. Laine, F.J. Vastola, J.P.L. Walker, J. Phys. Chem. 67 (1963) 2030–2034.
[31] C. Vix-Guterl, P. Ehrburger, in: P. Delhaes (Ed.), World of Carbon, Fibers and Composites, vol. 2, Taylor and Francis, Londres, 2003, pp. 188–218.
[32] N. Ab Manan, C. Hardacre, J. Jacquemin, D.W. Rooney, T.G.A. Youngs, J. Chem. Eng. Data 54 (2009) 2005–2022.
[33] R. Dennington, T. Keith, J. Millam, GaussView, Version 3.0, Semichem Inc., Shawnee Mission, KS, 2000–2003.

[34] R. Ahlrichs, TURBOMOLE User's Manual, Version 5.7, COSMOlogic GmbH & Co. KG, Leverkusen, Germany, 2004.
[35] A. Schafer, C. Huber, R. Ahlrichs, J. Chem. Phys. 100 (1994) 5829–5835.
[36] F. Eckert, A. Klamt, COSMOtherm User's Manual, Version C2.1,711 Release 01.08, COSMOlogic GmbH & Co. KG, Leverkusen, Germany, 2008.
[37] K.J. Miller, J.A. Savchik, J. Am. Chem. Soc. 101 (1979) 7206–7213.
[38] K.S.W. Sing, D.H. Everett, R.A.W. Haul, L. Moscou, R.A. Pierotti, J. Rouquerol, T. Siemieniewska, Pure Appl. Chem. 57 (1985) 603–619.
[39] D. Lozano-Castelló, E. Raymundo-Piñero, D. Cazorla-Amorós, A. Linares-Solano, M. Müller, C. Riekel, Carbon 40 (2002) 2727–2735.
[40] C. Matei Ghimbeu, R. Gadiou, J. Dentzer, L. Vidal, C. Vix-Guterl, Adsorption 17 (2011) 227–233.
[41] C. Matei Ghimbeu, R. Gadiou, J. Dentzer, D. Schwartz, C. Vix-Guterl, Langmuir 26 (2010) 18824–18833.
[42] V. Ruiz, C. Blanco, E. Raymundo-Piñero, V. Khomenko, F. Béguin, R. Santamaria, Electrochim. Acta 52 (2007) 4969–4973.
[43] Ph. Bernardo, J. Dentzer, R. Gadiou, W. Märkle, P. Novak, M.E. Spahr, C. Vix-Guterl, Carbon 49 (2011) 4867–4876.
[44] Y. Matsuda, T. Fukushima, H. Hashimoto, R. Arakawa, J. Electrochem. Soc. 149 (2002) A1045–A1048.
[45] V.P. Reddy, M.C. Smart, K.B. Chin, B.V. Ratnakumar, S. Surampudi, J.B. Hu, P. Yan, G.K.S. Prakash, Electrochem. Solid-State Lett. 8 (2005) A294–A298.
[46] J. Wang, X.-Q. Xie, T. Hou, X. Xu, J. Phys. Chem. A 111 (2007) 4443–4448.
[47] D.R. Lide, Handbook of Chemistry and Physics, 89th ed., CRC, 2008.
[48] C.O. Ania, J. Pernak, F. Stefaniak, E. Raymundo-Piñero, F. Béguin, Carbon 47 (2009) 3158–3166.